scientific reports

Check for updates

OPEN

Detection of caries lesions using a water-sensitive STIR sequence in dental MRI

Egon Burian[1,2,3]✉, Nicolas Lenhart[4], Tobias Greve[5], Jannis Bodden[1], Gintare Burian[6], Benjamin Palla[7], Florian Probst[8], Monika Probst[1], Meinrad Beer[2], Matthias Folwaczny[9] & Julian Schwarting[1]

In clinical practice, diagnosis of suspected carious lesions is verified by using conventional dental radiography (DR), including panoramic radiography (OPT), bitewing imaging, and dental X-ray. The aim of this study was to evaluate the use of magnetic resonance imaging (MRI) for caries visualization. Fourteen patients with clinically suspected carious lesions, verified by standardized dental examination including DR and OPT, were imaged with 3D isotropic T2-weighted STIR (short tau inversion recovery) and T1 FFE Black bone sequences. Intensities of dental caries, hard tissue and pulp were measured and calculated as aSNR (apparent signal to noise ratio) and aHTMCNR (apparent hard tissue to muscle contrast to noise ratio) in both sequences. Imaging findings were then correlated to clinical examination results. In STIR as well as in T1 FFE black bone images, aSNR and aHTMCNR was significantly higher in carious lesions than in healthy hard tissue ($p < 0.001$). Using water-sensitive STIR sequence allowed for detecting significantly lower aSNR and aHTMCNR in carious teeth compared to healthy teeth ($p = 0.01$). The use of MRI for the detection of caries is a promising imaging technique that may complement clinical exams and traditional imaging.

In clinical practice, carious lesions are detected based on inspection, instrumentation, and traditional radiographic imaging such as orthopantomogram (OPT) or bitewing radiographs[1,2]. Recent research has also shown that near-ultraviolet to near-infrared spectrum light can detect caries with increasing utilization in clinical settings[3,4]. Detection of caries by traditional radiographs relies on the demineralization of enamel or dentin, a late stage in the caries process. In the last decade, magnetic resonance imaging (MRI) and investigational sequences have become an attractive alternative in detecting carious lesions[5,6]. MRI could offer two significant benefits: first a reduction in radiation exposure, and second, the detection of carious lesions prior to traditional radiographic signs.

In a 2020 study by Cankar, the authors showed T2 mapping on MRI can detect pulpal reaction from penetration of caries into dentin[7]. In a 2015 systematic review by Schwendicke et al., radiographic caries detection was found more effective in advanced carious lesions, while alternative methods could be considered for initial carious lesions in populations with high caries risk or prevalence[2]. This conclusion highlights the limitation of traditional radiographic techniques, which are only capable of imaging carious lesions after enamel or dentin has been demineralized. The preceding steps, such as saliva penetration into porous tooth surface or reactive tertiary dentine formation, are concealed[8]. In 2001, Ekstrand et al. displayed the limited value of bitewing radiographs for incipient occlusal caries[9].

Recently, the literature on MRI sequences has substantially grown, and its application continues to expand. Technical progress, combined with the possibility of radiation-free imaging, greatly increased the interest in MRI

[1]Department of Diagnostic and Interventional Neuroradiology, Klinikum rechts der Isar, School of Medicine, Technical University of Munich, Munich, Germany. [2]Department of Diagnostic and Interventional Radiology, Universitätsklinikum Ulm, Ulm, Germany. [3]Department of Diagnostic and Interventional Neuroradiology, Kantonsspital Frauenfeld, Thurgau AG, Frauenfeld, Switzerland. [4]Department of Diagnostic and Interventional Radiology, Klinikum rechts der Isar, School of Medicine, Technical University of Munich, Munich, Germany. [5]Department of Neurosurgery, University of Munich, Munich, Germany. [6]Department of Prosthodontics, LMU University Hospital, Ludwig-Maximilians-University, Munich, Germany. [7]Department of Oral and Maxillofacial Surgery, University of Illinois, Chicago, Chicago, USA. [8]Department of Oral and Maxillofacial Surgery and Facial Plastic Surgery, University Hospital LMU Munich, 80337 Munich, Germany. [9]Department of Restorative Dentistry and Periodontology, LMU University Hospital, Ludwig-Maximilians-University, Munich, Germany. ✉email: e.burian@gmx.net

use in dentistry[10–15]. The scope of potential MRI applications in dentistry now covers a broad range, from wisdom tooth extraction, implant insertion, periodontal evaluation, and even orthodontics[16–20]. MRI has considerably better soft tissue contrast than radiation-based imaging techniques, and recently, its depiction of dental and osseous structures has become comparable to CT and CBCT with high dimensional stability[21–23].

The assessment of carious lesions using water-sensitive MRI sequences has not yet been performed. Since salivary penetration of dental hard tissue precedes demineralization and structure loss, early detection of pathological fluid concentration within dental hard tissue would be of high interest. The purpose of this study was to correlate carious lesions, as determined by dental radiographs and OPT, with findings on MRI sequences. A secondary aim was to assess the value of a water-sensitive Short tau inversions recovery (STIR) sequence in patients with clinically verified carious lesions.

Methods

Study design

This retrospective cohort study was designed in accordance with STROBE guidelines[24]. All 42 patients who presented at the Department of Periodontology, Ludwig-Maximilians-University Munich and received an MRI at the Department of Diagnostic and Interventional Neuroradiology, Klinikum rechts der Isar, Technische Universität München between October 2018 to April 2019, were retrospectively screened according to the following inclusion criteria:

1. Caries defined as the localized destruction of tooth structure according to Gibbons et al.[25], which can present as distinct surface changes of the enamel (brown and white lesions) or a cavitation in later stages, and can proceed to pulpal infection if not treated[26].
2. Imaging quality of Likert Grade ≥ 4 in the affected tooth

A consort scheme of patient inclusion is shown in Fig. 1. Patient characteristics are summarized in Table 1.

Clinical examination

All patients underwent standardized dental exam before imaging. Results were documented in standard fashion: Each tooth was categorized into 4 to 5 regions: Buccal, lingual, distal and mesial regions were documented for

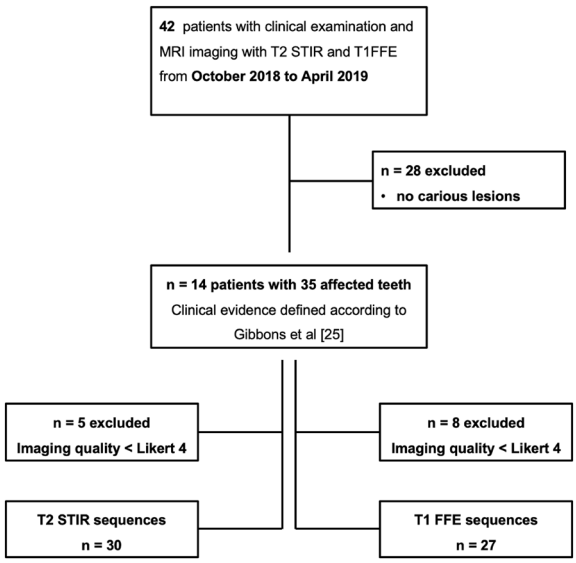

Figure 1. Flow chart shows patient recruitment.

Patient characteristics (n = 14)	
Age	52 (15)
Age range	20–71
Female	36%
Image quality (Likert grading scale)	4.44 (0.49)
Teeth excluded (artefacts) in STIR/T1 FFE	14% / 23%

Table 1. Patient characteristics. Data in parenthesis are SD.

every tooth. In premolars and molars, an occlusal region was also documented. In each region, fillings and/or the occurrence of carious lesions were documented.

MRI acquisition

All subjects were scanned with a 3T MRI scanner (Elition, Philips Healthcare, Best, The Netherlands) at the Department of Diagnostic and Interventional Neuroradiology, Technical University of Munich, using a 16-channel head-neck cervical spine array. Patients were positioned head-first in a supine position. The sequence protocol consisted of a short survey scan for sequence position planning (acquisition time 0:39 min), a three-dimensional (3D) isotropic short tau inversion recovery (STIR) sequence (acquisition time 6:03 min, acquisition voxel size $0.65 \times 0.65 \times 0.65$ mm^3, repetition time (TR) 2300 ms, echo time (TE) 184 ms, inversion recovery (IR) 250 ms, compressed sense, reduction 5, gap − 0.5 mm, slice oversampling 1.5, water-fat shift (pix)/bandwidth (Hz) 1766/246), and a 3D isotropic T1-weighted fast field echo (FFE) black bone sequence (acquisition time 5:31 min, acquisition voxel size $0.43 \times 0.43 \times 0.43$ mm^3, TR 10 ms, TE 1.75 ms, compressed sense, reduction 2.3, gap − 0.25 mm, water-fat shift (pix)/bandwidth (Hz) 1503/289).

Image analysis

Technical image quality was assessed using a 5-point Likert rating scale (1 = extremely poor, images are not clinically useful; 2 = poor, clinical use is not advised; 3 = average, borderline clinical use due to the image quality; 4 = good, containing no substantial adverse effect for clinical use; 5 = excellent, no restrictions for clinical use). Teeth were excluded from analysis if image quality was < Grade 4, which is defined as image quality with artifacts with little impact on image diagnosis, moderate sharpness and well distinguishable lesions with poorly defined edges[27].

All clinically affected teeth were included in the analysis. As healthy control, the correlating tooth in the opposite location in the same jaw (i.e., 27 for 17) was selected. If this tooth was extracted, affected by caries, or not analyzable due to image quality of Likert Grade < 4, the proximal tooth was used. 3D sequences were reconstructed in sagittal and coronal planes and aligned to the long axis for every tooth. As additional reference, muscular signal intensity was measured using the masseter muscle.

Apparent signal-to-noise ratios (aSNRs) and aHTMCNR (apparent Hard tissue – muscle contrast-to-noise ratio) were calculated in both sequences with mean signal intensities (SI) and standard deviations (SD) in the selected regions of interest (ROI). ROI conceptualization is exemplarily shown in Fig. 2. This methodology was adapted from measurements of nerve intensities as published for instance by Klupp et al.[28]:

$$aSNR\left(apparent\ signal\ to\ noise\ ratio\right) : SIhard\_tissue/SDdhard\_tissue$$

or

$$aSNR(apparent\ signal\ to\ noise\ ratio) : SIpulpa/SDpulpa$$

$$aHTMCDR(apparent\ hard\_tissue - muscle\ contrast\ to\ noise\ ratio) :$$

$$(SI\ hard\_tissue - SI\ muscle)/SD\ hard\_tissue$$

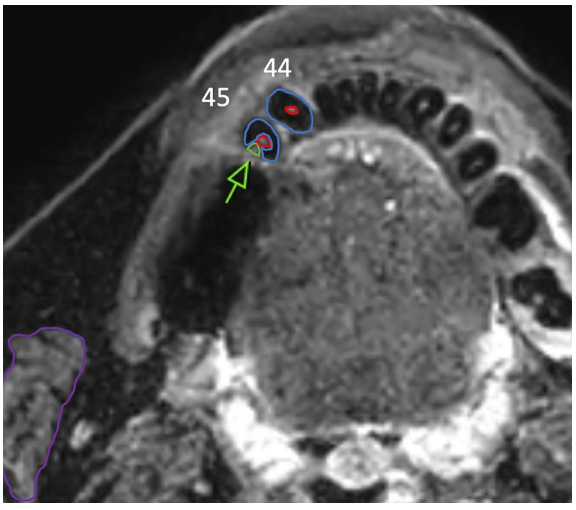

Figure 2. This figure illustrates the ROI placement in a STIR image in a carious tooth 45 and a healthy tooth 44. Purple: masseter muscle, green and arrow: carious lesion, red: pulp cavity, blue: dental hard tissue comprising enamel and dentin.

or

$$aHTMCDR(apparent\ pulpa - muscle\ contrast\ to\ noise\ ratio) :$$

$$(SI\ pulpa - SImuscle)/SDpulpa$$

Statistical analysis
Prism 9 (Graphpad Software LLC, Boston, United States) was used for all statistical tests. Normal distribution was tested using the Kolmogorov–Smirnov test. Wilcoxon matched pairs signed rank test was used to compare aSNR and aHTMCDR values. 20% of all values were tested for intrarater correlation by Pearson r test. P-values of < 0.05 were considered statistically significant.

Ethics approval and consent to participate
The study received institutional review board approval (Technical University of Munich: Ref.-No.185/18 S and Ludwig-Maximilians-University Munich: Ref.-No. 18-657). All participants gave written informed consent to the study. The authors confirm that all methods were carried out in accordance with relevant guidelines and regulations including the principles described in the Declaration of Helsinki.

Results
Patient cohort and clinical findings
Patient characteristics are summarized in Table 1. In this study, 14 patients with a total of 30 carious lesions met inclusion criteria.

Findings in T1 FFE sequences
All clinically suspected carious lesions were imaged using inverted T1 FFE sequences to create a CT-like image impression (Fig. 3). Due to susceptibility motion and metal artifacts reported for this sequence[29], 3 teeth were excluded due to poor image quality. Quantitative analysis using aSNR ratios showed no significant differences between the pulp of healthy and carious teeth ($p = 0.06$). Significant differences using aSNR ratios were detected between the dentin in healthy teeth and carious lesions ($p < 0.001$). Quantification using aHTMCNR also revealed significant differences between dentin in healthy teeth and carious lesions ($p < 0.001$). All remaining ratios were insignificant.

Findings in STIR sequences
In the STIR sequence, carious lesions presented as a hyperintensity compared to the surrounding healthy hard tissue (Fig. 3A–C). The STIR sequence also allowed for visualization of 25 proximal hyperintensities not detected clinically or in OPT (Fig. 4A–E). However, these findings were not statistically significant.

Further, carious lesions showed a high signal heterogeneity. There were significant differences in signal intensities using the aSNR ratios between the healthy tooth and carious esions ($p < 0.001$) as well as between the hard tissue and pulp in the carious and healthy teeth ($p = 0.03$ and $p = 0.02$ respectively). Comparisons of aHTMCNR ratios revealed a significant difference between pulp signal in carious teeth and healthy teeth ($p = 0.01$). Also, the signal to noise ratio of carious lesions was significantly higher than of healthy hard tissue ($p < 0.001$) (please see Tables 2 and 3).

Interreader agreement
Ratings were done by two independent, blinded readers. Interreader reliability was high ($r = 0.78$, $p < 0.001$).

Discussion
In this study, T1 based imaging identified statistically significant differences in signal intensities between hard tissue (comprising enamel and dentin) of healthy teeth compared to carious teeth. The results of this study validate prior work on T1 based imaging using ultra short echo times[5,30]. In addition, the use of a water-sensitive STIR sequence allowed for detecting significantly lower pulp signal to noise ratios in carious teeth but also significantly higher signal to noise ratios in carious lesions compared to healthy dental hard tissue. Another finding was, that signal intensities of carious lesions in STIR sequences were more heterogenous compared to T1. This observation could mirror the various levels of disease activity of in-vivo carious processes. However, it has to be stated that until today there are no reproducible and generally applicable rules to determine the precise level of activity within carious lesions. In dental offices clinical judgement and subjective measures are used, which are based on the dentists' experience. More active lesions harbor a moist, white surface with softer dental matrix, whereas arrested caries appears darker and harder[8,31].

Recent studies on the use of dental MRI has included fields of periodontology[10,16,32], endodontology[21,33], implantology[18,19], traumatology[34,35] and orthodontics[20]. Dental MRI has also investigated pulpal reactions to deeply penetrating carious lesions using ADC maps and T2 mapping, however, dentists have been skeptical regarding its clinical implementation[7,36,37]. With regard to image quality of the acquired images, the use of intra-oral coils specifically designed for dental applications allowed for taking a step further to optimizing diagnostic accuracy. Recently, the transition from regular MRI to dental dedicated MRI is fostered scientifically and clinically by Hilgenfeld et al. and Al-Haj Husain et al. showcasing the potential of the technique for different application fields like preoperative imaging and endodontics[21,22,38]. The lack of ionizing radiation associated with

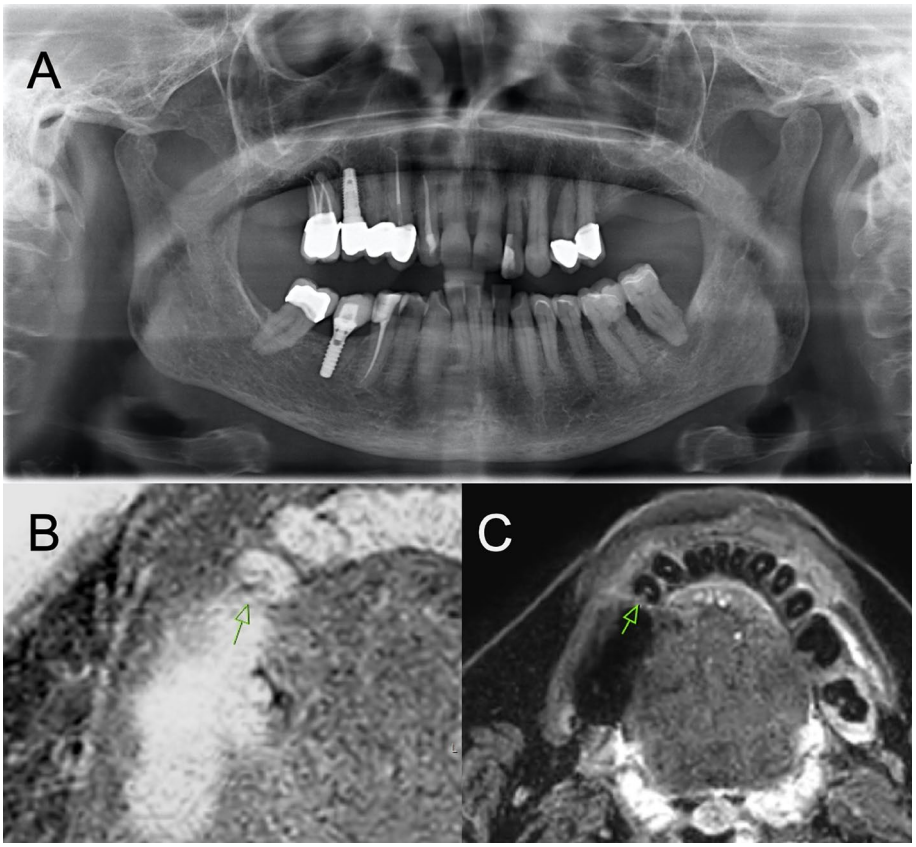

Figure 3. This figure shows a 67 years old female patient with multiple restorations. There are crowns inserted in 45 and 47 but also a titan implant in regio 46. These restorations cause metal artifacts in the corresponding region, but they do not hamper diagnostic accuracy with regard to the caries lesion distal in 44. (**A**) In the OPT a D4 carious lesion distal in the tooth 44 proximal to 45 can be detected, which also could be identified by clinical inspection. (**B**) The axial slice of the T1 FFE sequence shows a deep lesion located distally in 44 with association to the pulp cavity. Comparing to the STIR sequence depicted in C) the T1 FFE sequence is more prone to artifacts caused by metal restorations. C) The STIR sequence shows a hyperintesity with a similar configuration to the T1 based sequence. In both sequences the metallic artifacts caused by the implant placed in regio 46 and the prosthetic restorations do not hamper the diagnostic quality with regard to caries detection.

MRI has made it in extremely attractive alternative to traditional radiation-based imaging. Recent research has investigated the use of ultra-short echo time sequences to achieve a comparable spatial resolution like X-ray or CT using MRI, and thereby avoiding potential negative side effects of ionizing radiation[39–41]. The same efforts have been made recently in cariology, with the intent to generate images harbouring information similar to bitewing imaging or OPT[5,42].

The caries process has been studied since the fifteenth century, and it remains a critical interest in dental research today[43]. Although the bacterial toxin related decrease in pH and its induction of demineralization has been elucidated, the difference between active and arrested carious lesions remains a major issue in dental diagnostics today[8,9,25,26,44]. Clinically, caries detection is based on visual inspection of an air-dried lesion followed by palpation with a ball-ended explorer[26,44]. In meta-analyses the use of different activity indices has been evaluated, amongst which the International Caries Detection Assessment System (ICDAS) and Nyvad scoring system are the best known, and guide decision making on whether to excavate a carious lesion or not[26,44–46]. However, both of these scoring systems are based on clinician experience and evaluation, and therefore subjective assessments. In addition, proximal tooth lesions cannot be visually inspected, which increases the risk of missing subtle lesions. In these cases, bitewing radiographs are needed. However, as discussed above, these traditional imaging techniques cannot detect early caries process prior to demineralization[2]. There are recent scientific efforts investigating optical methods for the assessment of proximal carious lesions[3,4,47].

As displayed in this study, the use of a water-sensitive STIR sequence could be the newest addition to the armamentarium in the assessment of proximal carious lesions. In addition, our study found a high signal heterogeneity within the carious lesions, potentially mirroring different stages of activity associated with varying localized fluid leakage. The presented results and images allow for a first glimpse of what could be feasible in the future. However, prospective studies, including a larger cohort with clinical caries activity assessment and subsequent correlation with MRI are needed. The results of this study found that both sequences, the T1 gradient-echo

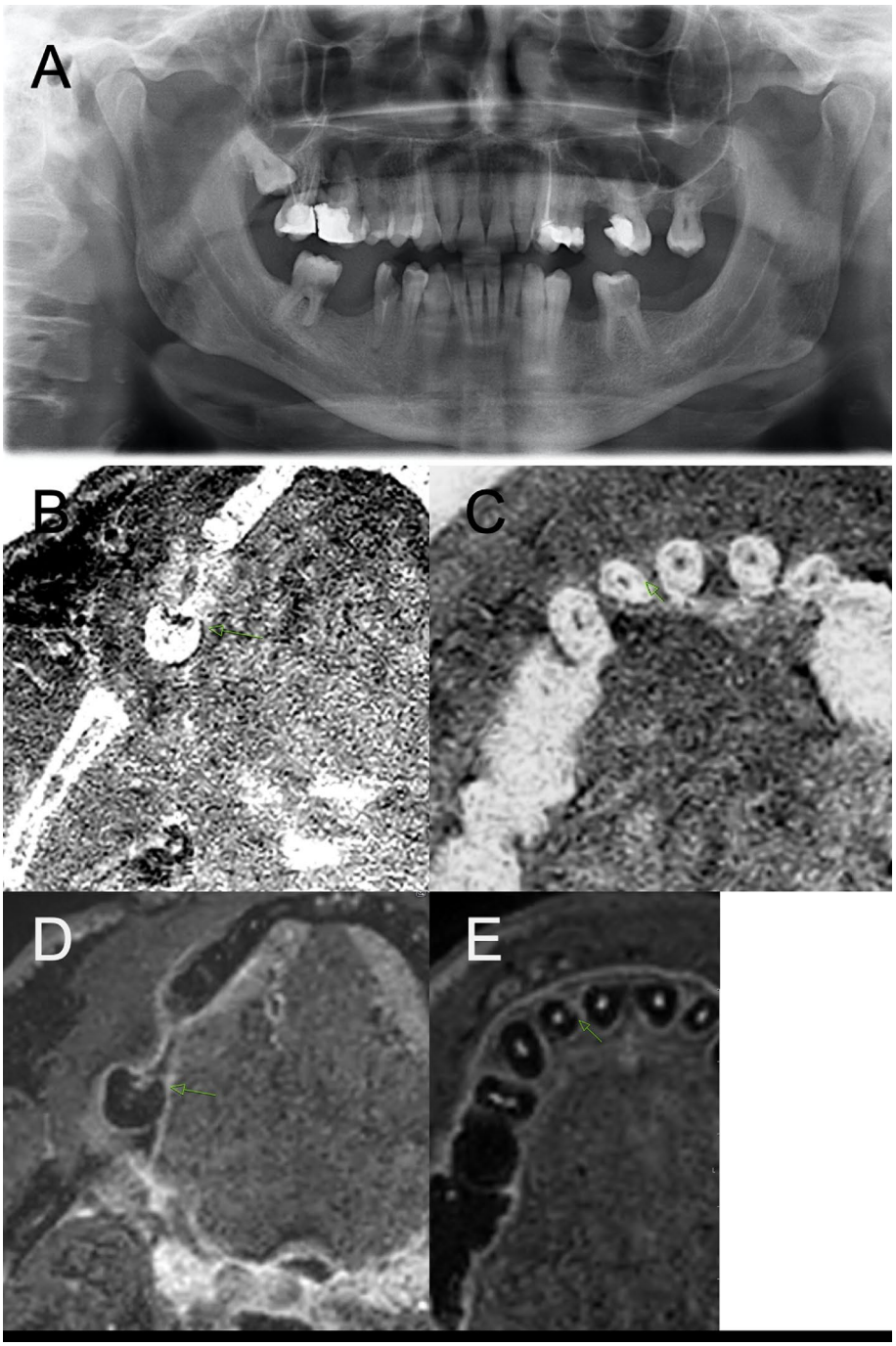

Figure 4. This figure shows a 40 years old male patients with multiple extensive carious lesions in the molar region of the mandible. (**A**) The OPT shows D4 carious lesions in the teeth 36 and 46 also detected clinically and verified by dental radiography (not shown). Also, a carious lesion can be detected in 44, which dispayed only a subte superficial lesion of the enamel but extensive destruction of the dentin. (**B**) In the T1 FFE sequence corresponding to the radiolucency a carious lesion is depicted in 46. (**C**) The STIR sequence also shows a localized hyperintensity with slightly minor dimension. With regard to the size of the carious lesion it can be assumed that only some areas maintain activity whereas some are already in an arrested state. (**D**) The 45° rotated tooth 12 shows no definite pathology neither in T1 based imaging nor in the OPT or clinical inspection. (**E**) In the STIR sequence a subtle localized hyperintensity is visualized in the mesial part of 12 and the gingival tissue between 11 and 12.

and the STIR sequence, allow for the detection of caries in vivo with good correlation to conventional imaging and inspection.

aSNR (n = 27)	Healthy tooth	Carious tooth	p
Hard tissue	3 [2, 4]	3 [2, 3]	0.63
Pulp	9 [6, 13]	9 [6, 14]	0.06
Carious lesion	–	4 [2, 6]	**< 0.001***
aHTMCNR (n = 27)			
Hard tissue	− 24 [− 29, − 12]	− 20 [− 29, − 12]	0.865
Pulp	− 1 [− 64, 0]	− 0 [− 3, 2]	0.29
Carious lesion	–	− 11 [− 15, − 6]	**< 0.001***

Table 2. Results of T1 FFE imaging. Data in parenthesis are IQR. *aSNR* apparent signal-to-noise ratio, *aHTMCNR* apparent hard tissue—muscle contrast-to-noise ratio. *Carious lesion vs. healthy hard tissue of the same tooth. Significant values are in bold.

aSNR (n = 30)	Healthy tooth	Carious tooth	p
Hard tissue	5 [5, 12]	5 [4, 6]	**0.03**
Pulp	17 [12, 33]	14 [10, 18]	**0.02**
Carious lesion	–	8 [5, 12]	**< 0.001**
aHTMCNR (n = 30)			
Hard tissue	− 16 [− 40, − 12]	− 14 [− 23, − 10]	0.10
Pulp	10 [7, 21]	9 [5, 12]	**0.01**
Carious lesion	–	− 8 [− 12, − 4]	**< 0.001**

Table 3. Results of STIR imaging. Data in parenthesis are IQR. *aSNR* apparent signal-to-noise ratio, *aHTMCNR* apparent hard tissue—muscle contrast-to-noise ratio. *Carious lesion vs. healthy hard tissue of the same tooth. Significant values are in bold.

This study has several limitations. First, the retrospective study design is prone to selection bias. Second, the small number of included patients does not allow for further conclusions with regard to the majority of patients. Third, no dedicated intraoral coil was used, which was reported before to have significant beneficial effects on image quality[21,22,33,38]. Further limitations are that MRI analysis was conducted on carious lesions detected on dental x-ray, the detection accuracy of MRI for dental caries has not yet assessed. The scanning time of the applied protocol was approximately 12 min, which is reduced greatly to less than 10 min by novel MR sequence protocols. Reducing the scan time is inherently associated with increasing image quality. Another limitation is, that the majority of lesions assessed by this study are severe carious lesions that can be detected clearly on dental x-rays. Furthermore, as shown by Fig. 4 there are lesions with a minor surface defect and a large deep carious lesion, which is easily identified by x-ray but is hardly detected using MRI. It also has to be mentioned, that metallic and movement artifacts can cause severe impairment of diagnostic quality in the applied sequence protocol reducing the number of included patients. Last, the retrospective nature of this study did not allow for correlation of pathological signal alterations in the MRI with supposedly negative clinical findings but only with x-ray records.

Conclusion

Using T1 gradient-echo and STIR sequences for caries detection was feasible and accurate in this clinical sample. The STIR sequence might offer advantages compared to conventional radiation-based dental imaging and clinical inspection with regard to detection of clinically asymptomatic lesions with unknown significance. Further prospective studies are needed to evaluate the use of water-sensitive MRI-sequences for early caries detection compared to visual inspection combined with x-ray imaging.

Data availability

All source data are stored at the Department of Neuroradiology, Technical University of Munich, Munich, Germany. We invite parties interested in collaboration and data exchange to contact the corresponding author directly.

Received: 1 July 2023; Accepted: 1 January 2024
Published online: 05 January 2024

References

1. Wenzel, A. Radiographic modalities for diagnosis of caries in a historical perspective: From film to machine-intelligence supported systems. *Dentomaxillofac. Radiol.* **50**, 20210010. https://doi.org/10.1259/dmfr.20210010 (2021).
2. Schwendicke, F., Tzschoppe, M. & Paris, S. Radiographic caries detection: A systematic review and meta-analysis. *J. Dent.* **43**, 924–933. https://doi.org/10.1016/j.jdent.2015.02.009 (2015).
3. Berghammer, K., Litzenburger, F., Heck, K. & Kunzelmann, K. H. Attenuation of near-ultraviolet, visible and near-infrared light in sound and carious human enamel and dentin. *Clin. Oral Investig.* **26**, 5847–5855. https://doi.org/10.1007/s00784-022-04541-7 (2022).

4. Lederer, A., Kunzelmann, K. H., Hickel, R. & Litzenburger, F. Transillumination and HDR imaging for proximal caries detection. *J. Dent. Res.* **97**, 844–849. https://doi.org/10.1177/0022034518759957 (2018).
5. Bracher, A. K. *et al.* Ultrashort echo time (UTE) MRI for the assessment of caries lesions. *Dentomaxillofac. Radiol.* **42**, 20120321. https://doi.org/10.1259/dmfr.20120321 (2013).
6. Tymofiyeva, O. *et al.* High-resolution 3D magnetic resonance imaging and quantification of carious lesions and dental pulp in vivo. *MAGMA* **22**, 365–374. https://doi.org/10.1007/s10334-009-0188-9 (2009).
7. Cankar, K., Vidmar, J., Nemeth, L. & Sersa, I. T2 mapping as a tool for assessment of dental pulp response to caries progression: An in vivo MRI study. *Caries Res.* **54**, 24–35. https://doi.org/10.1159/000501901 (2020).
8. Bjorndal, L. The caries process and its effect on the pulp: The science is changing and so is our understanding. *Pediatr. Dent.* **30**, 192–196 (2008).
9. Ekstrand, K. R., Ricketts, D. N. & Kidd, E. A. Occlusal caries: Pathology, diagnosis and logical management. *Dent. Update* **28**, 380–387. https://doi.org/10.12968/denu.2001.28.8.380 (2001).
10. Juerchott, A. *et al.* In vivo accuracy of dental magnetic resonance imaging in assessing maxillary molar furcation involvement: A feasibility study in humans. *J. Clin. Periodontol.* **47**, 809–815. https://doi.org/10.1111/jcpe.13299 (2020).
11. Ruetters, M. *et al.* Dental magnetic resonance imaging for periodontal indication: A new approach of imaging residual periodontal bone support. *Acta Odontol. Scand.* **77**, 49–54. https://doi.org/10.1080/00016357.2018.1499959 (2019).
12. Juerchott, A. *et al.* Comparison of non-contrast-enhanced dental magnetic resonance imaging and cone-beam computed tomography in assessing the horizontal and vertical components of furcation defects in maxillary molars: An in vivo feasibility study. *J. Clin. Periodontol.* **47**, 1485–1495. https://doi.org/10.1111/jcpe.13374 (2020).
13. Timme, M. *et al.* Imaging of root canal treatment using ultra high field 9.4T UTE-MRI: A preliminary study. *Dentomaxillofac. Radiol.* **49**, 20190183. https://doi.org/10.1259/dmfr.20190183 (2020).
14. Masthoff, M. *et al.* Dental Imaging: A basic guide for the radiologist. *Rofo* **191**, 192–198. https://doi.org/10.1055/a-0636-4129 (2019).
15. Pauwels, R. *et al.* Effective dose range for dental cone beam computed tomography scanners. *Eur. J. Radiol.* **81**, 267–271. https://doi.org/10.1016/j.ejrad.2010.11.028 (2012).
16. Probst, M. *et al.* Magnetic resonance imaging as a diagnostic tool for periodontal disease: A prospective study with correlation to standard clinical findings-Is there added value?. *J. Clin. Periodontol.* **48**, 929–948. https://doi.org/10.1111/jcpe.13458 (2021).
17. Valdec, S. *et al.* Comparison of preoperative cone-beam computed tomography and 3D-double echo steady-state MRI in third molar surgery. *J. Clin. Med.* **48**, 929–948. https://doi.org/10.1111/jcpe.13458 (2021).
18. Probst, F. A. *et al.* Magnetic resonance imaging based computer-guided dental implant surgery: A clinical pilot study. *Clin. Implant Dent. Relat. Res.* **22**, 612–621. https://doi.org/10.1111/cid.12939 (2020).
19. Hilgenfeld, T. *et al.* Use of dental MRI for radiation-free guided dental implant planning: A prospective, in vivo study of accuracy and reliability. *Eur. Radiol.* **30**, 6392–6401. https://doi.org/10.1007/s00330-020-07262-1 (2020).
20. Juerchott, A. *et al.* In vivo comparison of MRI- and CBCT-based 3D cephalometric analysis: Beginning of a non-ionizing diagnostic era in craniomaxillofacial imaging?. *Eur. Radiol.* **30**, 1488–1497. https://doi.org/10.1007/s00330-019-06540-x (2020).
21. Zidan, M. *et al.* Endodontic working length measurements of premolars and molars in high-resolution dental MRI: A clinical pilot study for assessment of reliability and accuracy. *Clin. Oral Investig.* **26**, 6765–6772. https://doi.org/10.1007/s00784-022-04636-1 (2022).
22. Hilgenfeld, T. *et al.* High-resolution single tooth MRI with an inductively coupled intraoral coil-can MRI compete with CBCT?. *Investig. Radiol.* **57**, 720–727. https://doi.org/10.1097/RLI.0000000000000890 (2022).
23. Probst, F. A. *et al.* Geometric accuracy of magnetic resonance imaging-derived virtual 3-dimensional bone surface models of the mandible in comparison to computed tomography and cone beam computed tomography: A porcine cadaver study. *Clin. Implant Dent. Relat. Res.* **23**, 779–788. https://doi.org/10.1111/cid.13033 (2021).
24. Vandenbroucke, J. P. *et al.* Strengthening the Reporting of Observational Studies in Epidemiology (STROBE): Explanation and elaboration. *Int. J. Surg.* **12**, 1500–1524. https://doi.org/10.1016/j.ijsu.2014.07.014 (2014).
25. Gibbons, R. J. & van Houte, J. Dental caries. *Annu. Rev. Med.* **26**, 121–136. https://doi.org/10.1146/annurev.me.26.020175.001005 (1975).
26. Braga, M. M., Mendes, F. M. & Ekstrand, K. R. Detection activity assessment and diagnosis of dental caries lesions. *Dent. Clin. North. Am.* **54**, 479–493. https://doi.org/10.1016/j.cden.2010.03.006 (2010).
27. An, H., Ma, X., Pan, Z., Guo, H. & Lee, E. Y. P. Qualitative and quantitative comparison of image quality between single-shot echo-planar and interleaved multi-shot echo-planar diffusion-weighted imaging in female pelvis. *Eur. Radiol.* **30**, 1876–1884. https://doi.org/10.1007/s00330-019-06491-3 (2020).
28. Klupp, E. *et al.* Improved brachial plexus visualization using an adiabatic iMSDE-Prepared STIR 3D TSE. *Clin. Neuroradiol.* **29**, 631–638. https://doi.org/10.1007/s00062-018-0706-0 (2019).
29. Fahlenkamp, U. L. *et al.* Advantages of a T1-weighted gradient-recalled echo (GRE) sequence with a radial 3D sampling approach versus 2D turbo spin-echo and cartesian 3D GRE sequences in head and neck MRI. *AJR* **214**, 747–753. https://doi.org/10.2214/AJR.19.21579 (2020).
30. Bracher, A. K. *et al.* Feasibility of ultra-short echo time (UTE) magnetic resonance imaging for identification of carious lesions. *Magn. Reason. Med.* **66**, 538–545. https://doi.org/10.1002/mrm.22828 (2011).
31. Bjorndal, L., Simon, S., Tomson, P. L. & Duncan, H. F. Management of deep caries and the exposed pulp. *Int. Endod. J.* **52**, 949–973. https://doi.org/10.1111/iej.13128 (2019).
32. Newbould, R. D., Bishop, C. A., Janiczek, R. L., Parkinson, C. & Hughes, F. J. T2 relaxation mapping MRI of healthy and inflamed gingival tissue. *Dentomaxillofac. Radiol.* **46**, 20160295. https://doi.org/10.1259/dmfr.20160295 (2017).
33. Juerchott, A. *et al.* Quantitative assessment of contrast-enhancement patterns of the healthy dental pulp by magnetic resonance imaging: A prospective in vivo study. *Int. Endod. J.* **55**, 252–262. https://doi.org/10.1111/iej.13662 (2022).
34. Feuerriegel, G. C. *et al.* Imaging of traumatic mandibular fractures in young adults using CT-like MRI: A feasibility study. *Clin. Oral Investig.* https://doi.org/10.1007/s00784-022-04736-y (2022).
35. Assaf, A. T. *et al.* Early detection of pulp necrosis and dental vitality after traumatic dental injuries in children and adolescents by 3-Tesla magnetic resonance imaging. *J. Craniomaxillofac. Surg.* **43**, 1088–1093. https://doi.org/10.1016/j.jcms.2015.06.010 (2015).
36. Cankar, K., Nemeth, L., Bajd, F., Vidmar, J. & Sersa, I. Discrimination between intact and decayed pulp regions in carious teeth by ADC mapping. *Caries Res.* **48**, 467–474. https://doi.org/10.1159/000358068 (2014).
37. Vidmar, J., Cankar, K., Nemeth, L. & Sersa, I. Assessment of the dentin-pulp complex response to caries by ADC mapping. *NMR Biomed.* **25**, 1056–1062. https://doi.org/10.1002/nbm.2770 (2012).
38. Al-Haj Husain, A. *et al.* Preoperative imaging in third molar surgery - A prospective comparison of X-ray-based and radiation-free magnetic resonance orthopantomography. *J. Craniomaxillofac. Surg.* https://doi.org/10.1016/j.jcms.2023.10.005 (2023).
39. Feuerriegel, G. C. *et al.* Diagnostic value of water-fat-separated images and CT-like susceptibility-weighted images extracted from a single ultrashort echo time sequence for the evaluation of vertebral fractures and degenerative changes of the spine. *Eur. Radiol.* **33**, 1445–1455. https://doi.org/10.1007/s00330-022-09061-2 (2023).
40. Schwaiger, B. J. *et al.* CT-like images based on T1 spoiled gradient-echo and ultra-short echo time MRI sequences for the assessment of vertebral fractures and degenerative bone changes of the spine. *Eur. Radiol.* **31**, 4680–4689. https://doi.org/10.1007/s00330-020-07597-9 (2021).

41. Huber, F. A. *et al.* Medication-related osteonecrosis of the jaw-comparison of bone imaging using ultrashort echo-time magnetic resonance imaging and cone-beam computed tomography. *Investig. Radiol.* **55**, 160–167. https://doi.org/10.1097/RLI.0000000000000617 (2020).
42. Weiger, M. *et al.* High-resolution ZTE imaging of human teeth. *NMR Biomed.* **25**, 1144–1151. https://doi.org/10.1002/nbm.2783 (2012).
43. Ruby, J. D., Cox, C. F., Akimoto, N., Meada, N. & Momoi, Y. The caries phenomenon: A timeline from witchcraft and superstition to opinions of the 1500s to today's science. *Int. J. Dent.* **2010**, 1–10. https://doi.org/10.1155/2010/432767 (2012).
44. Gimenez, T. *et al.* Visual inspection for caries detection: A systematic review and meta-analysis. *J. Dent. Res.* **94**, 895–904. https://doi.org/10.1177/0022034515586763 (2015).
45. Nyvad, B. & Fejerskov, O. Assessing the stage of caries lesion activity on the basis of clinical and microbiological examination. *Community Dent. Oral Epidemiol.* **25**, 69–75. https://doi.org/10.1111/j.1600-0528.1997.tb00901.x (1997).
46. Ismail, A. I. Visual and visuo-tactile detection of dental caries. *J. Dent. Res.* **83**, C56-66. https://doi.org/10.1177/154405910408301s12 (2004).
47. Litzenburger, F., Heck, K., Kaisarly, D. & Kunzelmann, K. H. Diagnostic validity of early proximal caries detection using near-infrared imaging technology on 3D range data of posterior teeth. *Clin. Oral Investig.* **26**, 543–553. https://doi.org/10.1007/s00784-021-04032-1 (2022).

Acknowledgements

We thank the study participants for their commitment to this study.

Author contributions

E.B. was responsible for the study conception and design, to data acquisition, to data analysis and interpretation, and to the writing and revision of the manuscript. J.S., N.L., N.S., T.G., J.B., G.B., B.P., F.P., M.P., M.B. and M.F. contributed to data acquisition, to data analysis and interpretation, and to the writing and revision of the manuscript. E.B., M.F. and J.S. contributed to the study conception and design, to data interpretation, and to the writing and revision of the manuscript. All authors reviewed and approved the final version of the manuscript and agreed to be accountable for all aspects of work ensuring integrity and accuracy.

Funding

Open Access funding enabled and organized by Projekt DEAL. MRI examinations of this project were covered by in-house funds of the Department of Diagnostic and Interventional Neuroradiology, Klinikum rechts der Isar, Technical University of Munich, Munich, Germany. The authors did not receive any other financial or material support.

Competing interests

The authors declare no competing interests.

Additional information

Correspondence and requests for materials should be addressed to E.B.